한국동력기계공학회지 제13권 제2호 pp.18~29 2009년 4월

Influence of Aspect Ratio on Friction Characteristics in Rectangular Gas Microchannel Flow
사각 미세채널 유동에서 마찰특성에 미치는 종횡비의 영향

M. T. Islam and Y. W. Lee
무하마드 타줄 이슬람·이연원

(received 5 November 2008, revised 28 January 2009, accepted 1 March 2009)

주요용어 : 누센수(Knudsen Number), 희박화(Rarefaction), 평균자유행로(Mean Free Path), 마찰계수(Friction Coefficient)

요 약 : 미세유동에 대한 폭발적인 관심에 의해 이 분야의 연구는 다양한 측면에서 이루어지고 있다. 본 연구는 사각 미세채널에서의 슬립유동에 관한 연구 중 아직 제대로 이루어져 있지 않은 마찰특성에 관한 종횡비의 영향에 초점을 맞추어 3차원 수치해석을 행하였다. 그 결과 종횡비가 1.0 일 때 상하 벽면 및 좌우측 벽면에서의 전단응력은 동일하나, 종횡비가 감소함에 따라 전단응력은 상하 벽면과 좌우측 벽면이 상이한 강도로 증가함을 보였다. 또한 Knudsen 수의 증가에 따라서는 전단응력이 감소함을 알 수 있었다. 따라서 벽면에서의 전단응력은 종횡비를 증가시키거나 혹은 Knudsen 수를 증가시키면 감소시킬 수 있으며, 마찰계수(fRe)도 종횡비를 증가시키거나 혹은 Knudsen 수를 증가시키면 감소됨을 밝혔다.

Nomenclature

AR : aspect ratio
D_h : hydraulic diameter [m]
f : Darcy friction factor
fRe : friction coefficient
H : channel height [m]
Kn : Knudsen number
n : normal coordinate on the channel wall [m]
p : pressure [Pa]
PR : pressure ratio (Pi/Po)
Pi : inlet pressure [Pa]
Po : outlet pressure [Pa]
R : gas constant [J/kg.K]
Re : Reynolds number
T : temperature [K]
u,v,w : velocity components [m/s]
u : cross sectional average velocity [m/s]
x,y,z : components of co-ordinate [m]

Greek symbols
λ : mean free path [m]
λ_s : coefficient of second kind of viscosity [N·s/ m2]
μ : dynamic viscosity [N·s/ m2]
μm : micrometer
ρ : density [kg/m3]
σ_T : energy accommodation coefficient
σ_m : momentum accommodation coefficient
τ_w : wall shear stress [Pa]

Subscript
i : channel inlet
o : channel outlet
1 : reference value

이연원(책임저자): 부경대학교 기계공학부
E-mail : ywlee@pknu.ac.kr, Tel : 051-629-6162
무하마드 타줄 이슬람: 부경대학교 대학원

1. Introduction

Nowadays microdevices are getting popularity all over the world because some of their attractive features like compact, more effective and easy to use. Microdevices are being used both for

commercial and scientific researches. The development of micromachining technology enables fabrication of micro-fluidic devices such as micro-valves, micro-pumps, micro-nozzles, micro-sensors, micro-heat exchangers etc. Microchannels and chambers are the essential parts of such devices. In addition to connecting different devices, microchannels are also used for reactant delivery as biochemical reaction chambers, in physical particle separation, in inkjet print heads, and as heat exchangers for cooling computer chips.

The surface to volume ratio for a machine with a characteristic length of $1m$ is $1m^{-1}$, while for a microdevice having a size of $1\mu m$ is $10^6 m^{-1}$. The million fold increase in surface area relative to the mass of the minute device substantially affects the mass, momentum and energy through the surface. Obviously surface effects dominate in microdevices [1]. As the surface area depends on aspect ratio so aspect ratio plays an important role on fluid flow and heat transfer in microgeometries. Friction characteristics in microgeometries are very important parameters to be known to design the microsystems effectively.

It is already established that the flow behavior in microgeometry is different from that of its macrocounterpart. There are two important effects in microgeometries such as compressibility and rarefaction. In the continuum limit, values of parameters at different points in the domain essentially represent average of the microscopic behavior in the neighborhood of the point. This assumption eventually leads to the formulation of the Navier-Stokes and energy equations as being the governing equations Beskok and Karniadakis[2]. However, these continuum equations those express conservation of mass, momentum and energy, breakdown for certain finite value of Knudsen number. The appropriate flow and heat transfer model depends on the range of Knudsen number. A classification of different flow regime is given by Schaaf[3] as follows:

i) For $Kn \leq 0.01$, the fluid can be considered as continuum.

ii) For $Kn \geq 10$, it is considered as free molecular flow.

A rarefied gas with Knudsen number between 0.01 and 10 can neither be considered as absolute continuum flow nor free molecular flow. In that region the flow is further classified into slip flow for $0.01 < Kn < 0.1$ and transition flow for $0.1 < Kn < 10$.

In the region of slip and early transition flow, velocity and temperature distributions in the flow field can still be determined from the Navier-Stokes and energy equations if velocity-slip and temperature-jump at the walls are taken into account.

Gaseous flows in long microducts have been studied by many authors. The experimental investigation on compressible gas flow through rectangular microchannels is difficult due to extraordinary small dimensions and associated complexity involved in it. In this regard numerical simulation may be treated as suitable.

P. Wu[4] performed experiments for both laminar and turbulent gas flow in microchannels. They used different trapezoidal cross sections with hydraulic diameters equal to 55.81, 55.92 and 72.38 μm. They observed that the measured friction coefficients were (10-30%) larger than those predicted by the conventional theory.

S. B. Choi[5] measured friction coefficient for a fully developed laminar flow using glass microtubes having diameters of 3, 7, 10, 53 and 81 μm with Reynolds numbers ranging from 30 to 20000. The tubes were very smooth with relative roughness of 0.0003. They found that the Poiseuille number was lower than the conventional value of 64.

D. Yu[6] conducted experiment through microtubes in silica having diameters of 19, 52 and 102 μm for Reynolds numbers ranging from 250 to 20000. They reported that the friction coefficients were lower than those measured by the conventional flow system. J. C. Harley[7] studied gas flow in silicon microchannels having

trapezoidal and rectangular cross sections of hydraulic diameters ranging from 1.01 to 35.91 μm. The aspect ratio varied between 0.0053 and 0.161. In this work they observed smaller friction coefficient with respect to the predicted conventional value.

T. Araki[8] investigated friction coefficients of nitrogen and helium through three different trapezoidal microchannels having hydraulic diameters ranging from 3 to 10 μm. The measured friction coefficients were smaller than the conventional values. They explained the reduced friction coefficient as the result of rarefaction effect.

J. Pfahler[9] measured the flow resistance of nitrogen and helium flow through silicon microchannels having hydraulic diameters ranging from 0.96 to 39.7 μm. The observed friction coefficients were smaller than those predicted by the conventional incompressible theory.

E. B. Arkilic[10] conducted analytical and experimental investigations into gaseous flow through long microchannels. A two- dimensional analysis of the Navier-Stokes equations with first order slip velocity boundary condition demonstrated that both compressibility and rarefaction effect were present in long microchannels. Using the equation of state of ideal gas, they showed that the zeroth order analytical solution for the streamwise mass flow corresponded well with the experimental results.

G. L. Morini[11] studied steady, hydro-dynamically developed, laminar flow in rectangular duct with first order slip boundary conditions. W. A. Ebert[12] studied a rarefied gas flow in rectangular duct with first order slip boundary conditions. C. S. Chen[13] proposed a numerical procedure for solving the reduced compressible Navier - Stokes equations with first order slip boundary conditions.

Although a lot of investigations have been performed by different researchers but the effect of aspect ratio on friction characteristics in rectangular microchannels has not been investigated yet. The objective of our investigation is to observe the influence of aspect ratio on friction characteristics of gaseous slip flow in rectangular micro- channels.

2. Model development

2.1 Problem statement

Nitrogen gas flow through three dimensional straight rectangular microchannels in Cartesian co-ordinate system is considered. Figurel shows the geometry and coordinate of the microchannel having the height, width and length are H, W and L respectively. Various aspect ratios (H/W, H W) from 1 (square) to 0 (parallel plate) are used to find their effect. The isothermal wall condition is considered with constant inlet gas and wall temperature at 310 K.

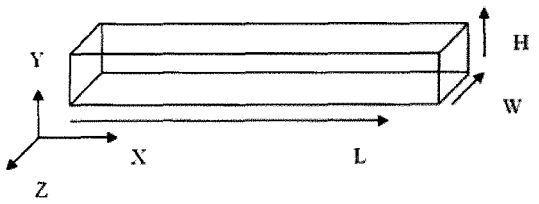

Fig. 1 Schematic diagram of the channel

2.2 Governing equations

The flow is governed by the three dimensional steady, compressible, constant viscosity Navier-Stokes equations. The governing equations are given below.

Continuity equation

$$\frac{\partial(\rho u)}{\partial x}+\frac{\partial(\rho v)}{\partial y}+\frac{\partial(\rho w)}{\partial z}=0 \tag{1}$$

Momentum equations

$$\rho u\frac{\partial u}{\partial x}+\rho v\frac{\partial u}{\partial y}+\rho w\frac{\partial u}{\partial z}= \tag{2}$$

$$-\frac{\partial p}{\partial x}+\mu\left[\frac{\partial^2 u}{\partial x^2}+\frac{\partial^2 u}{\partial y^2}+\frac{\partial^2 u}{\partial z^2}+\frac{1}{3}\left(\frac{\partial^2 u}{\partial x^2}+\frac{\partial^2 v}{\partial x\partial y}+\frac{\partial^2 w}{\partial x\partial z}\right)\right]$$

$$\rho u\frac{\partial v}{\partial x}+\rho v\frac{\partial v}{\partial y}+\rho w\frac{\partial v}{\partial z}= \tag{3}$$

$$-\frac{\partial p}{\partial y}+\mu\left[\frac{\partial^2 v}{\partial x^2}+\frac{\partial^2 v}{\partial y^2}+\frac{\partial^2 v}{\partial z^2}+\frac{1}{3}\left(\frac{\partial^2 u}{\partial x\partial y}+\frac{\partial^2 v}{\partial y^2}+\frac{\partial^2 w}{\partial y\partial z}\right)\right]$$

$$\rho u\frac{\partial w}{\partial x}+\rho v\frac{\partial w}{\partial y}+\rho w\frac{\partial w}{\partial z}= \tag{4}$$

$$-\frac{\partial p}{\partial z}+\mu\left[\frac{\partial^2 w}{\partial x^2}+\frac{\partial^2 w}{\partial y^2}+\frac{\partial^2 w}{\partial z^2}+\frac{1}{3}\left(\frac{\partial^2 u}{\partial x\partial z}+\frac{\partial^2 v}{\partial y\partial z}+\frac{\partial^2 w}{\partial z^2}\right)\right]$$

Energy equation

$$\rho c_p\left(u\frac{\partial T}{\partial x}+v\frac{\partial T}{\partial y}+w\frac{\partial T}{\partial z}\right) \tag{5}$$

$$=\left(u\frac{\partial p}{\partial x}+v\frac{\partial p}{\partial y}+w\frac{\partial p}{\partial w}\right)$$

$$+k\left(\frac{\partial^{2T}}{\partial x^2}+\frac{\partial^{2T}}{\partial y^2}+\frac{\partial^{2T}}{\partial z^2}\right)$$

$$+\mu\left(2\left(\frac{\partial u}{\partial x}\right)^2+2\left(\frac{\partial v}{\partial y}\right)^2+2\left(\frac{\partial w}{\partial z}\right)^2\right)$$

$$+\mu\left(\frac{\partial u}{\partial y}+\frac{\partial v}{\partial x}\right)^2+\mu\left(\frac{\partial w}{\partial y}+\frac{\partial v}{\partial z}\right)^2$$

$$+\mu\left(\frac{\partial w}{\partial x}+\frac{\partial u}{\partial z}\right)^2-\frac{2\mu}{3}\left(\frac{\partial u}{\partial x}+\frac{\partial v}{\partial y}+\frac{\partial w}{\partial z}\right)^2$$

The equation of state for ideal gas

$$p=\rho RT \tag{6}$$

The physical properties of nitrogen are given in Table 1.

Table 1 Physical constants of nitrogen

Parameters	value
Absolute viscosity μ	1.78×10^{-5} (N-s/m^2)
Specific gas constant R	296.009 (J/kg-K)
Ratio of specific heats γ	1.4

Stoke's hypothesis $\lambda_s+\frac{2}{3}\mu=0$ is used in momentum and energy equations which relates the first and second kind of viscosity[1].

3. Boundary conditions

3.1 Boundary conditions

The inlet and outlet are pressure boundary conditions with pressure ratio (Pi/Po)2 and outlet Knudsen number is 0.03 except stated otherwise. Velocity is considered uniform at the inlet i.e. at $x=0$, $\frac{\partial u}{dx}=0$ and $u=v=0$ and the inlet gas and wall temperature is fixed at $310\,K$. The slip velocity and temperature jump boundary conditions are imposed on the walls. Some cases are studied with no slip wall boundary conditions to compare the results and validate our simulations.

3.2 Slip wall boundary conditions

A user defined function(UDF) is used as subroutine to impose the slip boundary conditions on the walls. The slip boundary conditions are used as dimensionless form. The variables are made dimensionless as follows:

Velocities are normalized by the reference velocity u_1. The streamwise component x and its normal components y and z of the coordinate system are normalized by the channel length L and the channel hydraulic diameter D_h respectively. The mean free path λ, and temperature T are normalized by the channel height H and the reference temperature T_1 respectively. Cross sectional Reynolds number is defined by $Re=\frac{\bar{\rho}\bar{u}D_h}{\mu}$, where $\bar{u}$ and $\bar{\rho}$ are the cross sectional mean velocity and density respectively and $D_h=\frac{2*W*H}{W+H}$ is the hydraulic diameter of the channel.

The slip velocity boundary condition was proposed by Maxwell for an isothermal flow as

$$u_{gas}-u_{wall}=\frac{2-\sigma_m}{\sigma_m}Kn\frac{\partial u_s}{\partial n} \tag{7}$$

and the temperature jump boundary conditions by Von Smoluchowski as

$$T_g - T_w = \frac{2-\sigma_T}{\sigma_T}\left[\frac{2\gamma}{\gamma+1}\right]\frac{Kn}{\Pr}\frac{\partial T}{\partial n} \quad (8)$$

where $\left(\frac{\partial u_s}{\partial n}\right)$ and $\left(\frac{\partial T}{\partial n}\right)$ shows the variation of tangential velocity and temperature normal to wall [14]. The slip conditions expressed in (7) and (8) are in normalized form. The coefficients σ_m and σ_T are the tangential momentum and energy accommodation coefficients respectively. These two coefficients reflect the nature of tangential momentum and energy transfer between the impinging gas molecules and the solid walls. Very close to the wall, it can be assumed that half of the molecules are coming from the layer of the gas, one mean free path λ away, while other half of the gas are reflected from the wall[15]. In the current study it is considered that the hard sphere fluid particles collide with the solid walls diffusely, i.e. $\sigma_m = 1$ and $\sigma_T = 1$.

3.3 Numerical Method

The governing equations along with appropriate boundary conditions are solved by finite volume method using FLUENT. Second order upwind scheme is employed to discretize the nonlinear convective terms of the governing equations. SIMPLEC algorithm is used for pressure -velocity coupling in the flow field. As the domain is divided into small volume of hexahedral cells for calculation with the large number of meshes, a 16-node parallel computer is used for the simulations. Convergence criterion is set as normalized residual to 10^{-8} for energy equation and 10^{-6} for all other equations. Knudsen numbers are changed by changing the height of the channel and the related compressibility effects are considered and adjusted.

3.4 Grid independency test

To evaluate the grid size effect, grid independency tests are carried. To do this friction coefficients are evaluated for three different sizes of grid on a typical channel as shown in Table 2 and the results are compared.

Table 2 Grid independency test

Grid number	Reynolds number	Friction coefficient
21×21×1501	0.129265	45.782931
31×31×1801	0.125129	47.503584
41×41×2001	0.125075	47.504256

For a square microchannel with mesh numbers 21×21×1501 and 31×31×1801 the difference of cross sectional average friction coefficient is 3.76%. On the other hand with mesh numbers 31×31×1801 and 41×41×2001 that difference is on the order of 10^{-4}. Considering calculation time mesh number 31×31×1801 or its multiple are used according to the length of the dimensions of the domain. The maximum number of cells used in the current study is 3.8 million for the largest domain.

4. Result and Discussion

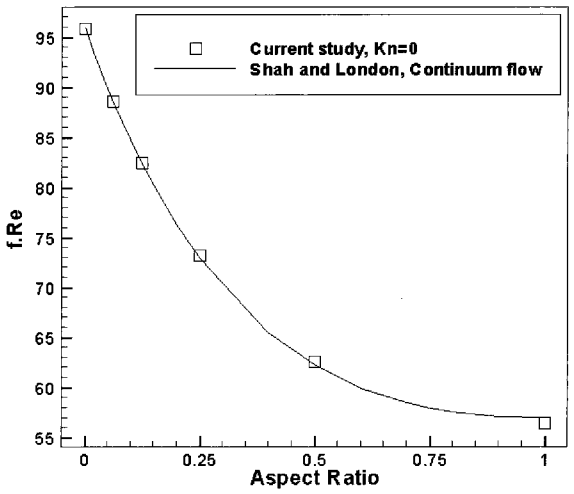

Fig. 2 Comparison of friction coefficient with that of Shah and London (1998)

At first several simulations are performed in conventional channels for different aspect ratios with noslip wall boundary conditions. These are performed to validate our noslip simulations by comparing friction coefficient with the reported friction coefficient in Shah and London[16]. The flows are assumed pressure driven with atmospheric outlet pressure and the pressure ratio is considered 2.5. For different aspect ratios

friction coefficients are evaluated and compared in Fig.2. The figure shows good agreement of the results. This comparison validates the simulation for no slip condition.

To validate the simulations of current slip flow model, the following simulations are conducted and compared with the corresponding experimental results.

Pressure distribution is compared with that of the experimental result reported by Pong et al.[17]. Simulations are conducted in a 3000 μm long, 40 μm wide and 1.2 deep microchannel with the same parameters as was used by Pong et al. and the comparisons are shown in Fig. 3. This figure shows that the pressure distribution for incompressible flow is linear because of constant density. For compressible flow the pressure distribution is nonlinear and the nonlinearity of pressure distribution for no slip model is higher than that of slip model. The pressure distributions agree well with those of Pong et al.

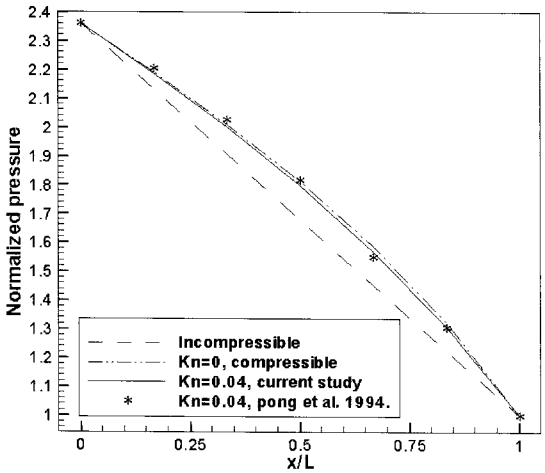

Fig. 3 Comparison of pressure distribution with Pong et al. (1994)

Mass flow rate data are compared with the experimental and analytical mass flow rate data reported by Arkilic et al.[18]. Arkilic conducted experimental and analytical investigation on helium flow through 1.33 μm deep, 52.25 μm wide and 7500 μm long microchannel at temperature 314 K. The accommodation coefficient was 1.1 and the inlet and outlet Knudsen numbers were 0.06 and 0.165 respectively.

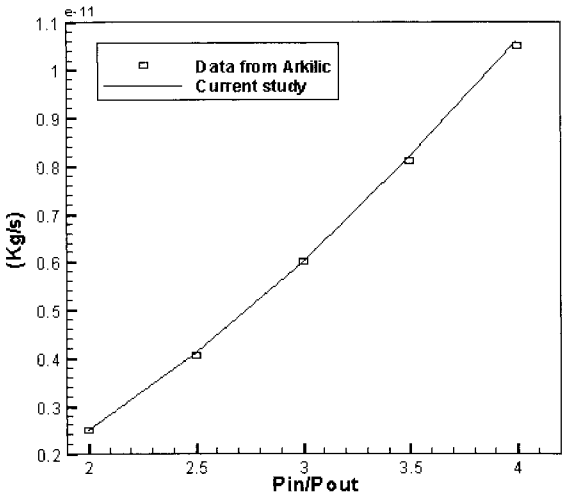

Fig. 4 Comparison of mass flow rate data with Arkilic et al. (1994)

To compare the result with that of Arkilic et al., simulations are performed with the same parameters as was used by Arkilic except tangential accommodation coefficient. Good agreement of mass flow rate data with that of Arkilic et al. are found when 1 is used as the accommodation coefficient in our simulations. The correlation is expressed by the Fig. 4.

The accommodation coefficients vary from 0 to 1. For most gas-surface interactions, the value of accommodation coefficient equal to 1 is the most appropriate choice (Arkilic et. al.)[19]. So the accommodation coefficients used by us are more reasonable.

The above comparisons validate the simulations of current study.

To investigate the effect of aspect ratio on wall shear stress, a series of simulations are carried out for different aspect ratios. Figure 5 shows the normalized wall shear stress distributions taken on the top/bottom walls. The figure exhibits that the wall shear stress increases with the distance from the inlet to the downstream location. This is because, as the fluid particles move to the downstream direction the velocity increases which is shown in Tajul and Lee[20]. As the velocity increases the wall shear stress also increases due to friction.

When the fluid flows then the side walls

experience friction for the motion of gas particles, as a result the pressure drops and density reduces. The reduction of density causes the increase of velocity as the law of continuity. The higher velocity further increases the shear stress and causes the pressure to drop further. So for the side walls density reduces and consequently the compressibility decreases. The compressibility and rarefaction are reciprocal, so when compressibility decreases then rarefaction increases. Consequently when the aspect ratio increases, the rarefaction effect of the channel also increases. The wall shear stress is reduced by the rarefaction due to wall slip. Hence wall shear stress decreases with the increase of aspect ratio which is displayed in Fig. 5.

The data used in Fig. 5 are tabulated in Table 3 to describe the result elaborately. Here the axial wall shear stresses on the top/bottom walls along the line $z = 0$ are denoted by τ_{tb} and the inlet wall shear by τ_i. Table 3 shows that when the aspect ratio is 1, then the normalized wall shear stress is 1.781. This value increases with the decrease of aspect ratio.

When the aspect ratio is 0.0625, the normalized wall shear stress is 1.844. The difference between the normalized wall shear stresses on top/bottom walls for aspect ratio 1 and 0.0625 is 3.48%.

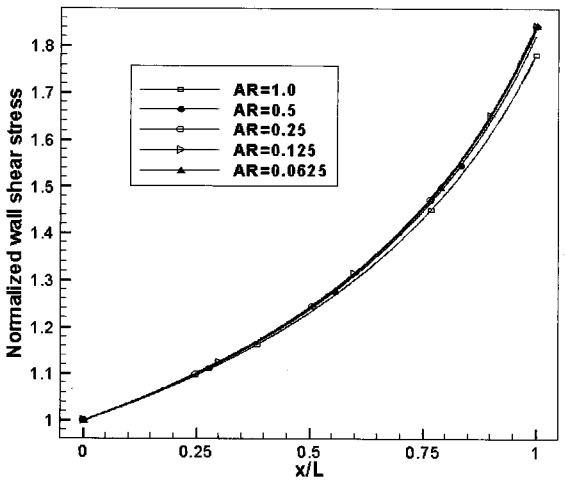

Fig. 5 Wall shear stress distribution along x axis on top/bottom walls, Kno=0.03

Table 3 Rate of decrease of wall shear stress on top/bottom walls for different aspect ratio

Aspect ratio AR_j	τ_{tb}/τ_i at outlet τ_j	$\left(\frac{\tau_j-\tau_{j+1}}{\tau_j}\right)\times 100$
1.0	1.781738	2.317
0.5	1.823021	0.9914
0.25	1.841094	0.61
0.125	1.84221	0.081
0.0625	1.843696	

Figure 6 shows the normalized wall shear stress distribution for different aspect ratios on the side walls. Like top/bottom walls, the wall shear stresses on side walls increase with the distance from the inlet to the downstream location.

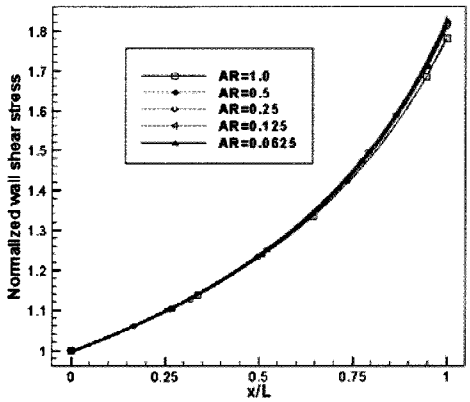

Fig. 6 Wall shear stress distribution along x axis on side walls, Kno=0.03

Table 4 Rate of decrease of wall shear stress on side walls for different aspect ratios

Aspect ratio AR_j	τ_{tb}/τ_i at outlet τ_j	$\left(\frac{\tau_j-\tau_{j+1}}{\tau_j}\right)\times 100$
1.0	1.781171	1.0256
0.5	1.79944	0.669
0.25	1.811484	0.3158
0.125	1.817206	0.273
0.0625	1.822168	

Also the wall shear stress increases for the decrease of aspect ratio. Like top/bottom walls, the wall shear stresses on the side walls decrease due to rarefaction. But the wall shear stresses on the side walls are lower than that of top/bottom walls.

This is because, as the aspect ratio increases, the rarefaction and consequently the wall slip velocity increases. Wall shear stress increases with the increase of velocity due to friction. The fluid velocity on the top/bottom wall is higher than that of side wall is already proved by Tajul and Lee[20]. As a result, the wall shear stress on the top/bottom wall is higher than those of side wall. From the figure it is clear that the wall shear stress decreases with the increase of aspect ratio. The minimum shear stress can be found when the aspect ratio is 1. So this study implies that the wall shear stress can be reduced by increasing aspect ratio. The data of this investigation are tabulated in Table 4. Here the axial wall shear stresses on the side walls, along the line $y=0$ are denoted by τ_{ss} and inlet wall shear stress is denoted by τ_i. The normalized wall shear stress for aspect ratio 1 is 1.781.

When the aspect ratio is 0.0625, the wall shear reaches to 1.822. The difference between the normalized wall shear stresses on side walls for aspect ratio 1 and 0.0625 is 2.30%.

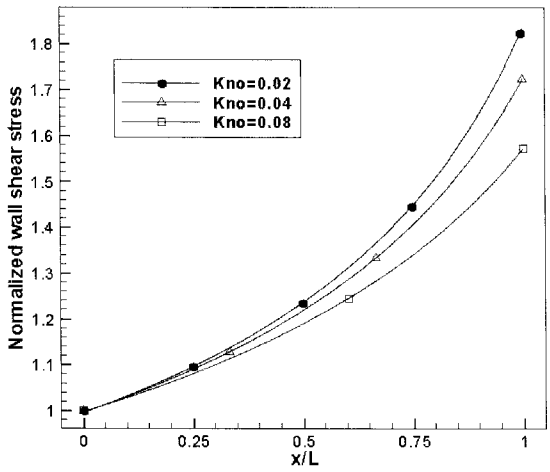

Fig. 7 Normalized wall shear stress for different Knudsen numbers, AR=1.0

According to Table 3 and Table 4, the normalized wall shear stresses on top/bottom and side walls are the same for aspect ratio 1. The difference of wall shear stresses on the top/bottom and side walls increases with the decrease of aspect ratio. The difference of wall shear stresses on the top/bottom and side walls is the maximum (1.181%) when the aspect ratio is 0.0625.

Figure 7 shows the normalized wall shear stress distribution for different Knudsen numbers. The wall shear stresses are normalized with the corresponding inlet value. The figure shows that as the Knudsen number increases the wall shear stress decreases. It results from the fact that when the Knudsen number increases then there is greater slip on the wall and consequently the flow resistance on the wall decreases. The value of the normalized wall shear stress at the outlet for Knudsen numbers 0.02, 0.04 and 0.08 are 1.83, 1.72 and 1.57 respectively. This finding implies that the wall shear can be reduced by increasing Knudsen number.

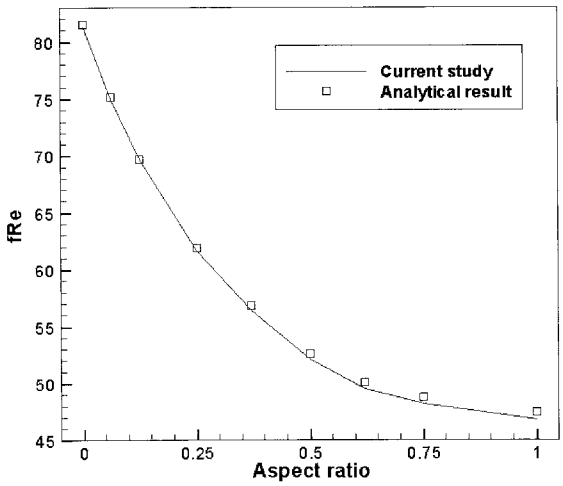

Fig. 8 Friction coefficient for different aspect ratios, Kno=0.03

The effect of aspect ratio on friction coefficient (fRe) is displayed by the Fig. 8. Due to the lacking of reported data, the current simulation result is compared with the analytical result. The analytical friction coefficient is evaluated as the product of Darcy friction factor $f=\frac{8\tau_w}{\bar{\rho}\bar{u}^2}$ and the Reynolds number $Re=\frac{\bar{\rho}\bar{u}D_h}{\mu}$. Here τ_w and $\bar{\rho}$ are the wall shear stress and cross sectional average density respectively. Cross sectional average slip velocity is evaluated by the following expression [21].

$$\bar{u}=\left(1+6\times\frac{2-\sigma_m}{\sigma_m}Kn\right)\times(1+\xi Kn)$$
$$\times\frac{W^2}{12\mu}\left(-\frac{dp}{dx}\right)\left[1-\frac{192\,W}{H\pi^5}\sum_{j-1,3,5\ldots}^{\infty}\frac{\tanh(j\pi H)}{j^5}\right].$$

Here is the local Knudsen number and ξ is a function of Kn for various aspect ratio ducts. The friction coefficient of current study for different aspect ratio agrees well with the analytical result. The figure shows that as the aspect ratio increases the friction coefficient decreases which is consistent to the result furnished in Fig. 6 and Fig. 7. In those figures wall shear stresses show the similar trend.

Figure 9 exhibits the friction coefficients for different Knudsen numbers for aspect ratios 1.0 and 0.5. It shows that the friction coefficient decreases with the increase of Knudsen numbers and the higher friction is observed in lower aspect ratios. The similar characteristics are found in previous figures. The friction coefficients ranges form 46.80 to 81.38 for decreasing values of aspect ratios from 1.0 to 0 for Knudsen number 0.03.

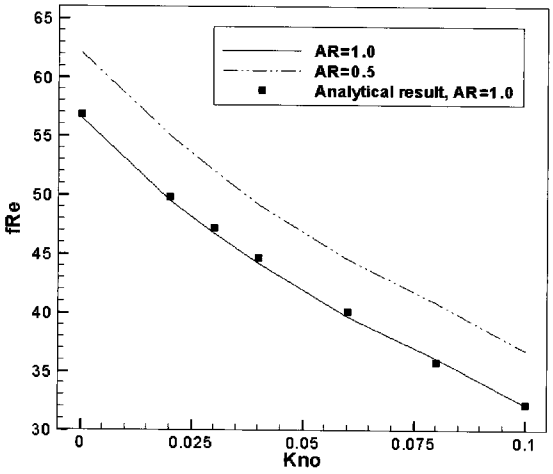

Fig. 9 Friction coefficient for different Knudsen numbers

Figure 10 shows the normalized pressure distribution for different aspect ratios. Ps indicates the pressure for slip boundary condition and Pns for no slip condition. For the effect of rarefaction, the pressure near the wall decreases and consequently the pressure drops. As a result the value of Pn/Pns is always less than unity.

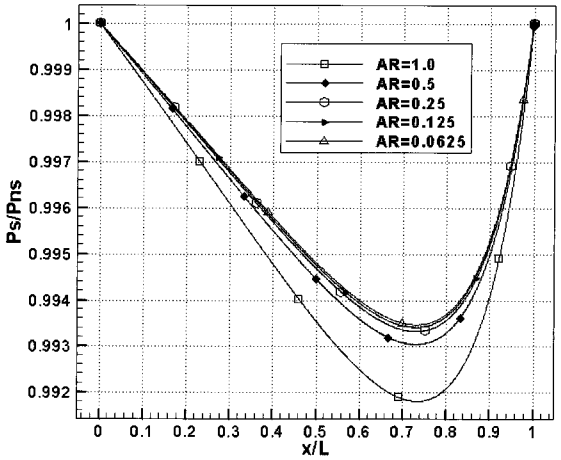

Fig. 10 Normalized pressure distribution for different aspect ratios

The fact that the rarefaction increases with the increase of aspect ratio and consequently the compressibility decreases has already been discussed. So when the aspect ratio is 1 then the rarefaction is the highest and the compressibility as well as the pressure nonlinearity is the lowest. According to the Fig. 3, pressure nonlinearity is the highest for no slip condition. Therefore the deviation of ratio Ps/Pns from the no slip pressure distribution is the highest when aspect ratio is 1. Consequently the maximum curvature is found in the curve which is related to aspect ratio 1. As the aspect ratio decreases the pressure nonlinearity of slip model increases and gets closer to the pressure distribution of no slip model. Hence the deviation of ratio Ps/Pns decreases and approaches to no slip pressure distribution. Therefore the figure shows decreasing curvature in the curves with decreasing aspect ratios.

Figure 11 shows the influence of outlet Knudsen number on the normalized mass flow rate. Here M* is the ratio of mass flow rate with slip condition over mass flow rate with noslip condition. It is found that M* is always greater than 1 which indicates that the slip mass flow rate is always greater than no slip mass flow rate. As the Knudsen number increases the slip velocity on the wall increases and wall shear stress decreases. As a result mass flow rate increases. Hence the mass flow rate increases with the increase of

Knudsen number but Knudsen number has no influence on the no slip mass flow rate. Therefore M* increases rapidly with the increase of Knudsen number. The value of M* increases from 1.098 to 1.15 for the increase of Knudsen number from 0.02 to 0.1.

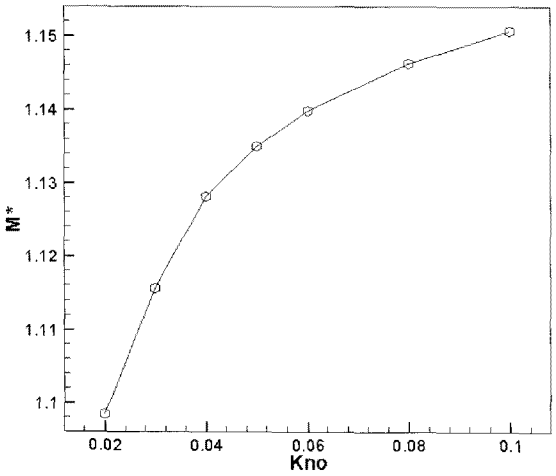

Fig. 11 Influence of Knudsen number on mass flow rate

Mass flow rate data of current study is also validated for different pressure ratios with that of Aubert and Colin et al.[22]. They used different pressure ratios with fixed outlet Knudsen number equal to 0.1. To compare with Aubert and Colin et al., simulations are performed with the same conditions as they did. Figure 12 shows the comparison of normalized mass flow rate data with the corresponding data reported in Aubert and Colin et al.

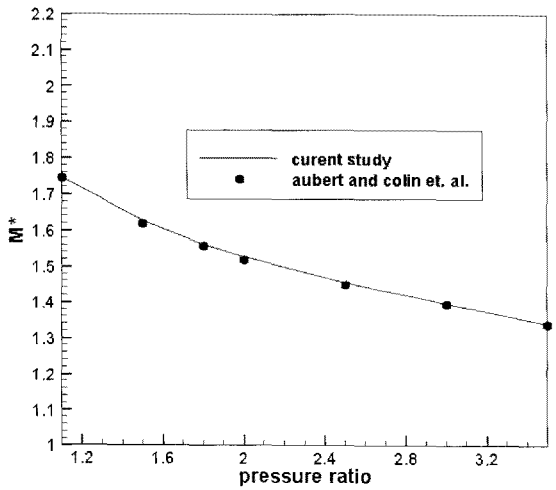

Fig. 12 Influence of pressure ratio on mass flow rate

The ratio of mass flow rate decreases with the increase of pressure ratio. This is due to the fact that as the pressure ratio increases the compressibility increases and rarefaction decreases. For the decrease of rarefaction, the rate of increase of slip mass flow rate decreases. But rarefaction has no influence on no slip mass flow rate. So the no slip mass flow rate increases with the increase of pressure ratio. As a result the ratio of slip mass flow rate over no slip mass flow decreases.

The friction coefficients (fRe) obtained from the slip and no slip conditions are compared in Table 5. From the table we see that the friction coefficient for slip condition is always lower than that of no slip condition. This is due to higher friction factor for no slip condition than that of slip condition. The table also shows that the friction coefficient increases with the decrease of aspect ratio.

Figure 13 shows the correlation between c* and aspect ratio where c* is the ratio of friction coefficient for slip condition over friction coefficient for no slip condition.

The figure shows that c* decreases with the increase of aspect ratio. This means that the rate of decrease of slip friction coefficient is higher than no slip friction coefficient and it is due to rarefaction effect. As the aspect ratio increases the rarefaction also increases which causes decrease of wall shear stress i.e. friction factor decreases and consequently the friction coefficient decreases rapidly for slip model. As a result the ratio of slip friction coefficient over no slip friction coefficient decreases with the increase of aspect ratio.

Table 5 slip and no slip friction coefficients for different aspect ratios

Aspect ratio	Slip friction coefficient, no=0.03	Noslip friction coefficient
1	46.80	57.24
0.5	52.09	62.12
0.25	61.63	72.96
0.125	69.67	82.55
0.0625	75.02	88.54
2D	81.38	95.90

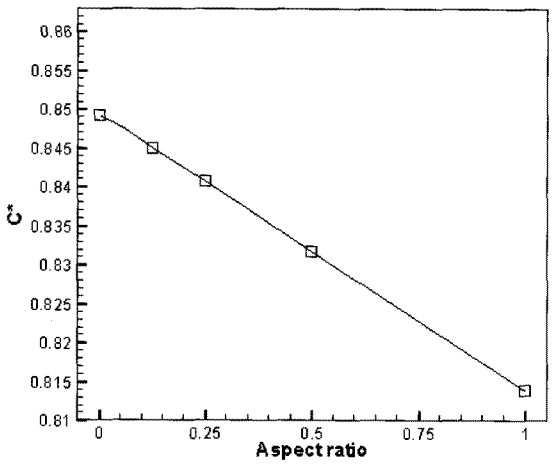

Fig. 13 Influence of aspect ratio on c*

5. Concluding remarks

Aspect ratio effects on friction characteristics are investigated in the current investigations. The wall shear stress increases with the decrease of aspect ratio. It is higher on the top/bottom walls than the side walls when aspect ratio is less than 1.0. As the aspect ratio increases this difference decreases. When the aspect ratio is 1.0 then the wall shear stress on the top/bottom and side walls are the same. Wall shear stress decreases with the increase of Knudsen number. We can conclude that the wall shear stress can be diminished by increasing aspect ratio or by increasing Knudsen number. Friction coefficient also decreases with increasing aspect ratio and increasing Knudsen numbers.

Acknowledgement

This work was supported by Pukyong National University Research Abroad Fund in 2005(PS-2005-018).

Reference

1. Gad-el-Hak, M., 2001, The MEMS Handbook, CRC press, New York.
2. A. Beskok and G. Karniadakis, 1994, "Simulation of heat and momentum transfer in complex microgeometries", Journal of Thermophysics and Heat Transfer, Vol. 8, No. 4, pp. 647~655.
3. S. A. Schaaf and P. L. Chambre, 1961, Flow of Rarefied gases, Princeton University Press, Princeton, NJ.
4. P. Wu and W. A. Little, 1983, "Measurement of friction factors for the flow of gases in very fine channels used for microminiature Joule-Thomson refrigerators", Cryogenics, Vol. 23, No. 5, pp. 273~277.
5. S. B. Choi, R. F. Barron and R. O. Warrington, 1991, "Fluid flow and heat transfer in microtubes", micromechanical sensors, Actuators, and systems, DSC ASME, New York, Vol. 32, pp. 123~134.
6. D. Yu et al, 1995, "An experimental and theoretical investigation of fluid flow and heat transfer in microtubes", Proceedings of ASME/JSME Thermal Engineering joint conference, Maui, HI, pp. 523~30.
7. J. C. Harley et al., 1995, "Gas flow in microchannels", J. Fluid Mech., Vol. 284, pp. 257~274.
8. T. Araki, M. S. Kim, H. Iwai and K. Suzuki, 2002, "An experimental investigation of gaseous flow characteristics in microchannels", Microscale Thermophysical Engineering, Vol. 6, pp. 117~130.
9. J. Pfahler et al, 1991, "Gas and Liquid Flow in Small Channels", Micromechanical Sensors, actuators and Systems, DSC ASME, New York, Vol. 32, pp. 49~60.
10. E. B. Arkilic, M. A. Schmidt and S. B. Kenneth, 1997, "Gaseous Slip Flow in Long Microchannles", Journal of Microelectromechanical Systems, Vol. 6, No. 2, pp. 167~178.
11. G. L. Morini and M. Spiga, 1998, "Slip flow in rectangular microtubes", Microscale Thermophysics. Eng., Vol. 2, pp. 273~282.
12. W. A. Ebert and E. M. Sparrow, 1965, "Slip flow in rectangular and annular ducts", J. Basic Eng., Vol. 87, pp. 1018~1024.

13. C. S. Chen, 2000, "Numerical method for predicting three-dimensional steady compressible flow in long microchannel", J. Micromech. Microeng., Vol. 14, pp. 1091~1100.
14. R. W. Barber and D. R. Emerson, 2006, "Challenges in modeling gas-phase flow in microchannels: From slip to Transition", Heat Transfer Engineering, Vol. 27, No. 4, pp. 3~12.
15. P. H. Oosthuizen and W. E. Carscallen, 1997, Compressible fluid flow, McGraw-Hill companies, Inc., pp. 464~479.
16. R. K. Shah and A. L. London, 1998, Laminar flow forced convection in ducts, Academic Press, New York.
17. K. C. Pong, et al, 1994, "Non-linear pressure distribution in uniform microchannels", ASME-Publications-FED, Vol. 197, pp. 51~56.
18. E. B. Arkilic, S. B. Kenneth and M. A. Schmidt, 1994, "Gaseous flow in micro-channels", FED Application of Micro-fabrication to Fluid Mechanics ASME, Vol. 197, pp. 57~66.
19. E. B. Arkilic, S. B. Kenneth and M. A. Schmidt, 2001, "Mass flow and tangential momentum accommodation in silicon micromachined channels", J. Fluid Mech., Vol. 437, pp. 29~43.
20. Md. Tajul and Y. W. Lee, 2007, "Effect of Aspect Ratio on Gas Microchannel Flow", Journal of KSPSE, Vol. 11, No. 3, pp. 16~21.
21. G. Karniadakis and A. Beskok, 2002, Micro Flows: Fundamentals and simulation, Springer-Verlag, New York.
22. C. Aubert and S. Colin, 2001, "Higher-order boundary conditions for gaseous flows in rectangular microducts", Micro-scale Thermophysical Engineering, Vo. 5, pp. 41~54.